Proceedings of ASME Turbo Expo 2022
Turbomachinery Technical Conference and Exposition
GT2022
June 13-17, 2022, Rotterdam, The Netherlands

GT2022-82248

EXPERIMENTAL AND NUMERICAL CHARACTERIZATION OF THE SELF-EXCITED DYNAMICS BEHAVIOR OF A TECHNICALLY PREMIXED BURNER

R. Meloni*, S. Gori, G. Riccio
Baker Hughes
Florence, 50127, Italy
Email: roberto.meloni@bakerhughes.com

N. Chiarizia, D. Pampaloni, A. Andreini
Department of Industrial Engineering, DIEF,
University of Florence,
Florence, 50139, Italy

ABSTRACT

In this paper, the numerical findings of a high fidelity CFD model will be compared with the experimental data of a test campaign devoted at characterizing the performance of a technically premixed industrial burner regarding the thermo-acoustic instabilities.

The data are retrieved at relevant gas turbine conditions in a test bench where the flame tube can change its length during the test execution allowing its fundamental acoustic frequencies to be modified and, in case, triggered. Mimicking the test configuration, several Large-Eddy Simulations are performed with different lengths of the flame tube in order to verify the ability of the numerical model to reproduce the excited dominant frequency and the corresponding limit cycle amplitude measurements. Th

e numerical model demonstrates the ability to correctly reproduce the frequency triggered during the test and to reach different limit cycle amplitudes along different flame tube lengths in agreement with the tests, as well. However, it is found that the amplitude of the acoustic pressure fluctuation during the limit cycle is generally under-predicted. Despite this, the proposed approach demonstrates to be a robust tool for the characterization of a given design, allowing to dramatically reduce the computational cost of the analysis, at least in the early design phase.

Since the numerical model can correctly reproduce the behavior of the investigated design, a deep post-processing of the solutions is performed to shed light on the physical mechanisms sustaining the thermo-acoustic instability. Among the numerical techniques employed at this purpose, the Phase-Locked Average and the Extended-POD are applied trying to correlate the fluctuations of the different quantities inside the premixed channel of the burner and the primary zone as well.

NOMENCLATURE

Symbols

A	Model constant	
c	Speed of sound	[m/s]
c	Filtered progress variable	
C_s	Dynamic-Smagorinsky Constant	
f_D	Dominant Frequency	[Hz]
f_n	Fundamental harmonics	[Hz]
G	Stretch Factor	[-]
L	Flame Tube length	[m]
L_o	Minimum flame tube length	[m]
l_t	Sub-grid length scale	[m]
l_{int}	Integral length scale	[m]
n	Mode number	[-]
p’	Acoustic pressure	[Pa]
T	Temperature	[K]
u	Velocity	[m/s]
u'	Turbulent velocity fluctuation	[m/s]
U_l	Laminar flame speed	[m/s]
U_t	Turbulent flame speed	[m/s]
Z	Mixture fraction	

*Address all the correspondence to this author

Greek

α	Thermal diffusivity	[m^2/s]
Δ	Filter length	[m]
ϕ	Equivalence ratio	[-]
$\dot{\omega}_c$	Progress variable source	[kg/m^3s]
ρ	Density	[kg/m^3]
∇	Gradient operator	[-]
τ	Convective time	[s]

Subscripts

D	Dominant referred to frequency
l	Laminar
t	Turbulent
u	unburnt

Acronyms

BOI	Body of Influence
CFD	Computational Fluid Dynamics
CFL	Courant-Friedrichs-Lewy
DLN	Dry-Low NOx
FFT	Fast-Fourier Transform
FGM	Flamelet Generated Manifold
FTT	Flow-Through Time
ISO	International Standards Organization
GT	Gas Turbine
LES	Large Eddy Simulation
mmf	Mean Mixture Fraction
PDF	Probability Density Function
POD	Proper Orthogonal Decomposition
RS	Reference size of the grid
SED	Self-Excited Dynamics
SGS	Subgrid scale

INTRODUCTION

Combustion dynamics represent the most limiting factor for the operability of the Dry-Low NO_x (DLN) systems for Gas Turbines (GT) combustors based on lean premixed flames [1-4]. In normal operation, the reduction of the pollutant emissions could be compromised by the rising of the thermo-acoustic instabilities due to the leaner and leaner premixed regime the engines have to deal with. Additionally, in extreme cases, these instabilities could even lead to the shutdown of the unit, with a consequent reduction of the life of the mechanical components subjected to severe temperature gradients. In the power generation and, more importantly, in the oil and gas sector, the design of a burner is even more challenging from this standpoint [5]. The fluctuation of the fuel gas composition as well as the sudden variations in loads the engine has to perform to follow the power demand can dramatically change the behavior of the unit.

So, the characterization of the performance of a design solution with respect to the thermo-acoustic instabilities is a step that needs to be anticipated quite early during its development phase [6-8]. At this purpose, several numerical methods have been proposed over the last decades, aiming also at reducing the extremely high experimental costs related to this kind of investigation [9]. The generation of the Flame Transfer Function (coupled with an acoustic solver) correlating the flame response to small perturbations of the acoustic field, is the most used approach [10-12]. Unfortunately, this method is not able to predict the non-linear effects and provide reliable and accurate information about the limit cycle saturation. On the other side, the non-linearity between the heat release rate and the acoustic could be captured by the calculation of the Flame Describing Function where perturbations at different levels of amplitude are considered [13-16]. However, the complexity of the approach and even the high computational cost required to run several high fidelity Large-Eddy or Stress-Blended Eddy Simulations limited the diffusion of this methodology. It must be also noticed that the use of these numerical findings for design purposes should also be supported by a detailed validation phase against experiments [15]. Instead, in literature, there has been little direct comparison [18-19] and, in the most of cases, it is limited to lab-scale tests or not relevant operating conditions .

An alternative methodology rising in the last years is represented by the use of compressible LES for the investigation of the Self-Excited Dynamics of a GT combustor [20-21]. The chance to execute a virtual test including all the design details of the system or exactly replicate a given operating condition represents the main advantages. Furthermore, such kind of practice, joint with advanced post-processing techniques, could also be used to provide a deep physical understanding of the mechanism (self-) sustaining the instability, leading to potential modifications and improvements of the design [22-26]. Nevertheless, a quite exhaustive understanding of the behavior of a system against parameters like the fuel composition or other design and operability constraints is computationally unaffordable, especially for industrial-scale applications [27].

From both experimental and numerical point of view, a solution able to contain the costs providing an exhaustive preliminary characterization of a design against the combustion dynamics is offered by the exploitation of the “so-called” thermo-acoustic rigs [28]. The latter has the capability to execute the tests in a *“single-burner”* configuration while performing a detailed screening of the excitable frequencies by dynamically changing the length of the combustor. Numerically, the replication of this approach allows a dramatic reduction of the size of the models that have to be run along different flame tube lengths to investigate a design solution. Despite some important aspects like the flame-to-flame interaction could be neglected, the investigation of the self-excited dynamics through this strategy can represent a powerful compromise, especially at the beginning of a new product development.

In the present paper, the numerical validation of a test campaign performed leveraging such kind of test article topology will be presented. The content of the work will start with the description of the experimental apparatus, pointing the focus on how the screening of the excitable frequencies is executed and providing information about the main data that will be used during the validation phase. Then, the description of the

numerical model will be proposed both in terms of combustion model and computational domain. The latter involves not only the mimicking of the test rig but also the strategy of simulating different lengths of the combustor for the triggering of the instabilities. In the last section, the investigation will focus on the application of some advanced post-processing algorithms to some unstable conditions, trying to detect the physical mechanism sustaining the feedback between the unsteady heat release and the acoustic field.

TEST ARTICLE AND PREMIXER DESIGN TOPOLOGY

A simplified overview of the thermo-acoustic rig exploited to execute the experimental test campaign is reported in Figure 1. The pressurized combustion air flow is metered and controlled upstream the burner independently of the air flow passing through the sleeve for the cooling of the flame tube walls. The operating pressure of the test article as well as the temperature of the oxidizer can be modulated in order to mimic different operating conditions of the gas turbine cycle, such as part loads, cold/hot day conditions, etc. Referring to the test conditions that are investigated in this work, the operating pressure is equal to the full pressure at the ISO base load conditions of the NOVA LT® family axial compressor. Furthermore, the facility allows for the proper control of the fuel composition so that, even the impact of this critical parameter onto the triggering of the self-excited dynamics can be fully investigated.

The core of the rig is represented by a mobile piston installed at the end of the flame tube, controlling also the counter-pressure of the entire system. During the test, the position of the piston head can be varied at constant velocity along the flame tube, so as to change the acoustic length of the chamber.

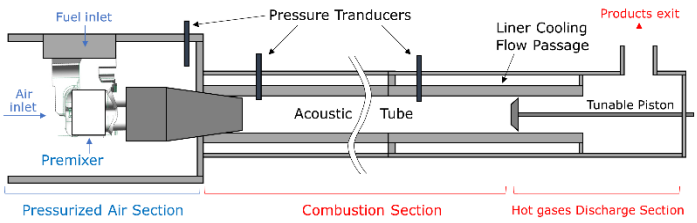

Figure 1. *Thermo-acoustic rig: the mobile piston can dynamically change its own position during the test varying the acoustic frequencues of the flame tube. © 2022 Baker Hughes Company - All rights reserved.*

Assuming a *closed-closed* configuration from the acoustic standpoint, for a given flame tube L, the tube is characterized by the following fundamental harmonics:

$$f_n = n\frac{c}{2L} \quad (1)$$

being c the speed of sound. So, the characterization of a design and the detection of the frequencies that it is able to trigger at specific operating conditions can be performed by a sweep of the mobile piston position. While this screening can be done in a quite fast manner, once the positions of the piston head exciting specific frequencies have been detected, the test can be also repeated at those positions while maintaining the piston head fixed, acquiring the data for longer time and higher frequency resolution.

The rig is equipped with several pressure transducers installed along the combustor walls: the corresponding signals can be used for the re-construction of the mode shape of the excited tones. From the numerical perspective, the first pressure probe downstream the premixer will be taken as reference for the comparison of the numerical results against the data. Obviously, all the additional quantities measured during the test and concurring to the definition of the boundary conditions of the numerical model have been used in this work, like the temperature at the different locations of the liners.

Regarding the burner, a technically premixed solution is investigated in this work. In terms of pollutant emissions, such design is able to meet the single digit target for both NO_x and CO [29]. The achievement of a mixture with a low degree of unmixedness at the inlet section of the combustor is guaranteed by:

- a strong interaction between the combustion air and the fuel injected in cross flow, enhancing the mixing among the reactants;
- an optimized length of the premixing duct.

Figure 2 shows the non-dimensional mean mixture fraction radial profile at the exit of one of the 4 tubers forming the premixer. The level of un-mixedness, calculated considering the maximum and the minimum of the fuel concentration along the radial span, is estimated equal to 5% only. This profile and the corresponding contour plot reported in Figure 2 are time-averaged from one of the simulation performed during the investigation.

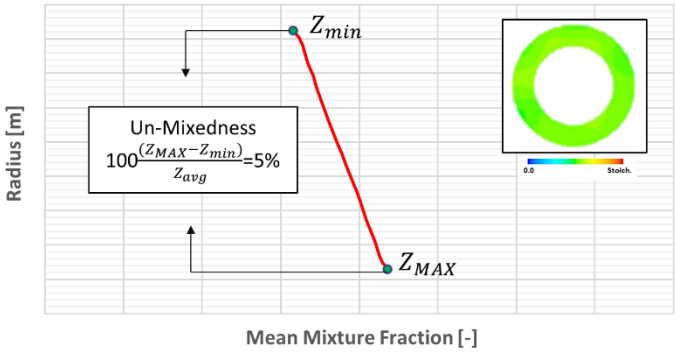

Figure 2. *Circumferential average profile of the mean mixture fraction at the exit of one of the 4 tubers forming the premixer with the corresponding countour plot and un-mixedness level. © 2022 Baker Hughes Company - All rights reserved.*

The diameter of the fuel injecting holes in the numerical model is assumed at the nominal value. This choice could potentially and theoretically influence the results, especially in terms of amplitude of the triggered mode. Further considerations about this aspect will be formulated in the Results and Discussion section.

NUMERICAL MODELLING

In this paragraph, the main aspects related to the numerical process will be presented. Firstly, the combustion model adopted along the LES turbulence closure is discussed. Then, the attention will focus on the simulated computational domain and the corresponding mesh resolution, especially inside the premixer. Lastly, the key information about the numerical setting will be provided.

Combustion and Sub-Grid Models

The pre-tabulated combustion model FGM [31] with non-adiabatic energy treatment embedded into the commercial code Ansys Fluent 18 is used in this paper. So, the thermo-chemical state is expressed as a function of the mean mixture fraction Z and the progress variable c. Dealing with hydrocarbon fuels, the latter parameter is expressed considering the mass fraction of CO and CO_2 along the premixed flamelet configuration [30]. The GRI-Mech3.0 is selected as chemical kinetic mechanism. The assumed Probability Density Function (PDF) to treat the sub-grid turbulence-chemistry interaction, based on standard beta function, includes the compressibility effects of the gases, being a critical parameter to be accounted for when the coupling between the heat release rate and the acoustic field has got to be captured. The density is calculated according to the PDF-option available in Fluent.

The sub-grid scale (SGS) source term of the progress variable transport equation $\dot{\omega}_c$ is expressed according to the turbulent flame speed closure, as follows [32-33]:

$$\overline{\dot{\omega}_c} = G\rho_u U_t |\nabla \tilde{c}| \quad (2)$$

with ρ_u the density of the unburnt and G the stretch factor kept to the value of 1. The turbulent flame speed is computed according to Eq. 3, considering the SGS velocity fluctuation u' and the thermal diffusivity α:

$$U_t = A(u')^{3/4} U_l^{1/2} \alpha^{-1/4} l_t^{1/4} \quad (3)$$

The laminar flame speed of the mixture U_l is calculated using the opposite premixed flame configuration in Cantera [34] at the same operating condition of the test. The sub-grid length scale l_t is formulated according to the dynamic-Smagorinsky theory:

$$l_t = C_s \Delta \quad (4)$$

where C_s is a constant of the model evaluated run time during the simulation and Δ is the grid filter length.

The model constant A (equal to 1.5) is kept constant for all the cases that will be presented in this paper. No preliminary study was performed to optimize this model parameter.

Regarding the LES closure at the walls, the default wall functions are employed.

Computational Domains and Mesh resolution

The computational domain and specifically the length of the flame tube (calculated as the burner exit-to-piston distance) has been changed in agreement with the simulated test conditions. Eight different test rig configurations are simulated independently, so that 8 different static grids are generated: further details will be provided in the Results and Discussion paragraph where the experimental conditions will be provided.

Mass flow inlet type boundary condition is employed for both the combustion air and the fuel. The plenum located upstream the premixer is included also in the numerical model allowing the turbulent flow to be fully developed inside the burner. The pressure outlet of the domain is characterized by an effective passage area and an imposed pressure drop ensuring that the section is chocked, in agreement with the test conditions. These choices ensure that the acoustic boundary conditions are correctly reproduced by the numerical model. The annular passage of the cooling air is not implemented to limit the cell count, especially for the cases with the longest flame tube: the temperature distribution at the liner walls is imposed according to the recorded experimental values.

The computational polyhedral grids are generated following the same criteria for each simulated test condition. The finest mesh resolution is applied to the fuel line and the premixer volumes where the Reference Size (RS) of the mesh is applied. Additionally, Bodies of Influence (BOIs) are specified for the primary zone of the combustor and for the cross-flow regions where the fuel is injected, creating an even more dense mesh. A coarser mesh is adopted further downstream the flame tube while an even rougher grid is created in the upstream plenum. Figure 3 provides a general overview of the mesh size at the different regions.

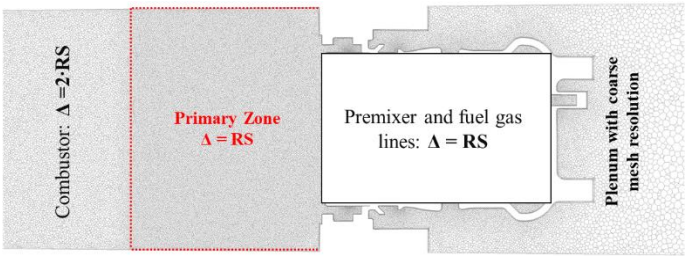

Figure 3. *Mesh resolution along the different regions of the computational domain.*

This strategy allows the gradient of the main quantities to be properly captured at each location, like the temperature distribution influencing the heat release rate inside the primary zone and the mixture fraction governing the mixing in the premixing duct. At this purpose, Figure 4-Top shows an instantaneous field of the mixture fraction super-imposed to the grid downstream a fuel gas hole. From this picture, it can be seen that the channel is discretized with more than 30 cells. Considering the half of the channel height as a measure of the integral length scale l_{int}, such discretization guarantees that the LES is able to resolve approximately 90% of the turbulent kinetic energy spectrum even at the high Reynolds number associated to the pressurized conditions at which the tests are executed. Moreover, Figure 4-Bottom reports the Pope's index [35-36] at the fuel injection location and further downstream the premixing duct, demonstrating that the above mentioned turbulent kinetic

energy content can be resolved with the adopted discretization. Basing on this findings, it has been decided not to perform any mesh sensitivity study.
The same discretization strategy is employed for all the 8 computational grids that will be discussed later on the paper: the overall cell count is 18 million polyhedral cells for the case with the shortest flame tube length and about 40 million for the longest one, respectively.

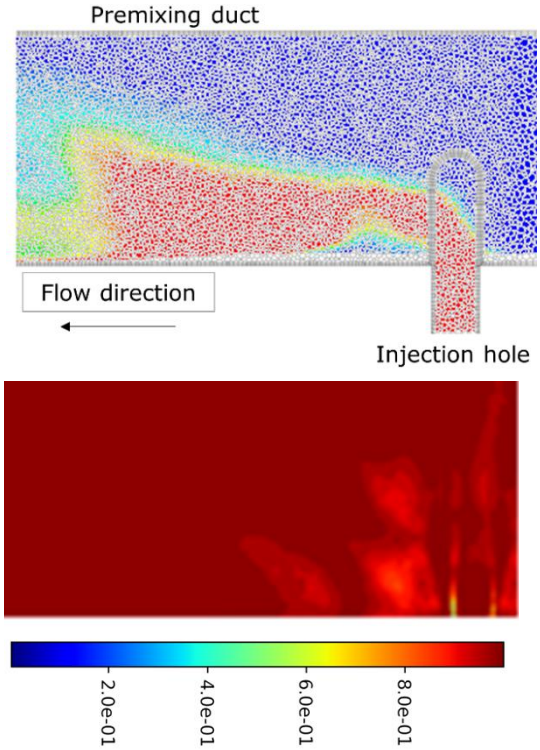

Figure 4. Top: *Polyhedral grid close up in the region of the fuel injection. The effect of the local refinement due to the BOI is visible in the right hand side of the figure upstream the injection hole.* ***Bottom****: Pope Index calculated at the fuel injection location.*

Numerical Setting

Considering the highest mesh resolution the domain has been discretized with, the time step size is calculated in order to maintain the CFL number below the unity. The time step size has order of magnitude of o(-6), and it is kept fixed along the simulation. The second order implicit scheme is employed for the temporal discretization. The QUICK scheme is used for all the other equations with the exception of the pressure and the density for which the second order upwind is employed and for the momentum equation, discretized through the bounded central differencing.

As for the solution strategy, for the cases showing a thermo-acoustic instability, the time-average phase is enabled after that the solution has reached the numerical convergence (i.e., the wash-out phase is completed) and after that the limit cycle saturation is reached, performing the sampling for about 4 FTTs of the flame tube. For the triggered frequencies, this sampling time ensures the recording of a high number of cycles. For the cases affected by noise or very weak pressure oscillation, the solution is washed-out for 4 FTTs and sampled for 3 FTTs.

RESULTS AND DISCUSSION

The operating conditions analyzed in this study refer to a test campaign aiming to characterize the above described design at the cycle of a typical small size heavy-duty GT. More specifically, a piston sweep at *full speed-full load* condition of the NOVA LT16® GT is here considered. The tests are executed in this way: a first sweep is performed with the piston moving slowly but constantly to search for the instabilities. Once the lengths triggering the combustion instabilities have been detected, the data are acquired with the piston at fixed position to avoid any transient effects. The pre-heated combustion air temperature mimics a *new-and-clean* compressor working with ISO ambient conditions. The firing temperature is kept constant as well as the pressure drop across the premixer so that only the impact of the acoustic property change onto the thermo-acoustic behavior of the system can be isolated. The tests are executed with pure methane as fuel gas. Even if the performance can be largely affected by the fuel composition, this choice represents a good compromise between gas rich in C_{2+} and gas with high inert.

Figure 5 summarizes the experimental tests results in the so-called water fall diagram where the triggered frequencies and the corresponding pressure fluctuation amplitudes are reported as a function of the dome-to-piston distance. Regarding the latter parameter, the flame tube length ranges between about $1.5L_0$ and $2.5L_0$ (being L_0 the minimum combustor length), practically covering the entire range of excitable frequencies a gas turbine combustor can experience.

The analysis of the experimental data shows that the self-excited frequencies fall in a narrow range across the dominant frequency f_D, namely from $0.94\ f_D$ to $1.05\ f_D$, generating a sort of sloped island for the mode that is progressively triggered. This behavior means that different modes are excited while the dominant frequency is not subjected to significant changes. According to Eq. 1, the dashed curves super-imposed in Figure 5 represent the acoustic frequencies of the mode i^{th} at the different flame tube lengths calculated through this equation.

So, what the experimental data highlight is that, increasing the dome to piston distance, the premixer excites preferentially the same dominant frequency along different mode shapes. So, for example, when the tube has a length between $1.7L_0$ to $2.0L_0$, the dominant frequency is triggered by the 4^{th} longitudinal mode, while for higher flame tube lengths the same frequency is excited by the 5^{th} mode. The length of the flame tube also influences the amplitude of the pressure fluctuation. Firstly, there are some ranges of this parameter producing no excitation of the acoustic field (i.e., between $1.65L_0$ and $1.70L_0$): on the water-fall diagram this produces the presence of well identifiable isolated islands. Additionally, looking more in detail to what happens inside a single island, it can be noticed that the amplitude is

subjected to a first rise increasing the tube length. Once the peak is reached, a further increase produces a drop in amplitude. Such behavior cyclically repeats along the entire diagram.

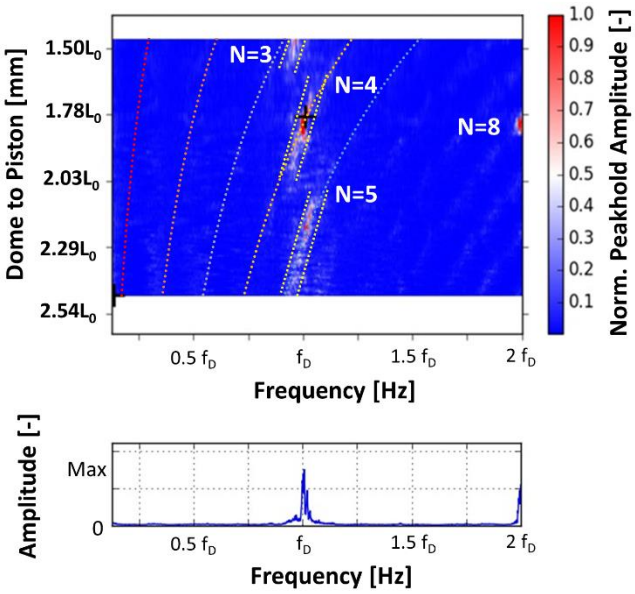

Figure 5. *Experimental water fall reporting the map of the frequencies triggered varying the dome-to-piston distance and the corresponding amplitudes. For the case with the highest pressure pulsation amplitude, the FFT is reported. © 2022 Baker Hughes Company - All rights reserved.*

Focusing the attention on the test data obtained with the dome-to-piston distance at around $1.8L_0$, it can be observed that there is one exception regarding the excited frequencies. In these conditions, the acoustic pressure of the dominant frequency reaches a so high level that also the second harmonic, corresponding to the $N = 8$ mode at $2\,f_D$ is triggered. The bottom part of Figure 5 reports the FFT of this specific operating condition showing that also this harmonic reaches a level of amplitude close to the maximum.

Five different configurations are considered for the validation of the numerical results. They are summarized in Table 1 where the normalized values of the dominant frequency and the amplitude are reported for each case. The normalization is performed against the peak amplitude value, recorded, as mentioned before, with a piston-to-dome distance of $1.8L_0$.

Table 1. *Selected flame tube configurations for the numerical study: the experimental values of the amplitude are normalized against the maximum experimental fluctuation recorded at* $1.8\,L_0$ *of flame tube length. © 2022 Baker Hughes Company - All rights reserved.*

	Piston to Dome distance [mm]				
	$1.6L_0$	$1.8L_0$	$2.0L_0$	$2.2L_0$	$2.4L_0$
f_D	$1.04\,f_D$	f_D	$1.05\,f_D$	$1.02\,f_D$	$0.94f_D$
Amplitude	0.25	1	0.15	0.65	0.15
Triggered mode	-	4	-	5	-

Once the model has been validated, 3 additional configurations have been simulated to test the behavior of the model out of the experimental range. Further information about them will be provided later on the next sections.

Numerical Findings: Validation Cases

Figure 6 mimics the experimental water-fall diagram for the selected operating conditions. The size of the bubbles corresponds to the normalized amplitude of the instability. For consistency, the normalization is done considering the same experimental peak value.

The numerical results show that, in terms of dominant frequency, the model is in perfect agreement with the data since the change of frequency as a function of the flame tube length is correctly reproduced. In absolute terms, a small drift is obtained regarding the numerical dominant frequency against the experimental value for all the flame tube lengths: to quantify this typical discrepancy, the FFT of the case with $1.8L_0$ (reported in the bottom side of the picture) shows a difference in terms of frequency of -2.5% with respect to the data.

Analogously to the experiments, the amplitude of the instability is sensible to the dome-to-piston distance as well. The right-hand side graph of Figure 6 better highlights this dependency: the interpolation of the pressure amplitudes shows a sort of sine wave demonstrating that the cyclic behavior described in the previous paragraph is perfectly reproduced. Looking at the amplitudes of the instability, it can be seen that the self-excited model is also able to reproduce the absolute peak with the tube length at $1.8L_0$. A slightly lower amplitude is reached at $2.2L_0$.

Looking at the numerical amplitudes, it can be observed that the model provides an under-prediction if compared to the experimental values. For example, for the same condition where the maximum value of the amplitude is reached, the model covers only the 35% of the experimental pressure fluctuation. The under-estimation of the amplitude has also the consequence that the frequency associated to the $N = 8$ mode is not triggered. Typically, these secondary modes are excited only when the amplitude of the triggered frequency is very high (like happened during the tests), a condition that is not reproduced numerically. Instead, a good agreement is reached when the amplitude is quite far from the peak, like for tube lengths of $1.6L_0$ and $2.0L_0$.

There could be several reasons why the numerical model is not able to perfectly reproduce the amplitude of the limit cycle when the instability is significant. The highest uncertainty, according to the authors' opinion, can be associated to the ability of the model to capture the flame position and, consequently, to describe the heat release rate properly. This aspect is crucial especially for perfectly premixed flames characterized by long flames and quite homogeneous heat release distributions. The inclusion of the effect of strain in the flame brush description could potentially bring a benefit since it has been demonstrated that it provides improvements in the prediction capability of the combustion model [37-38].

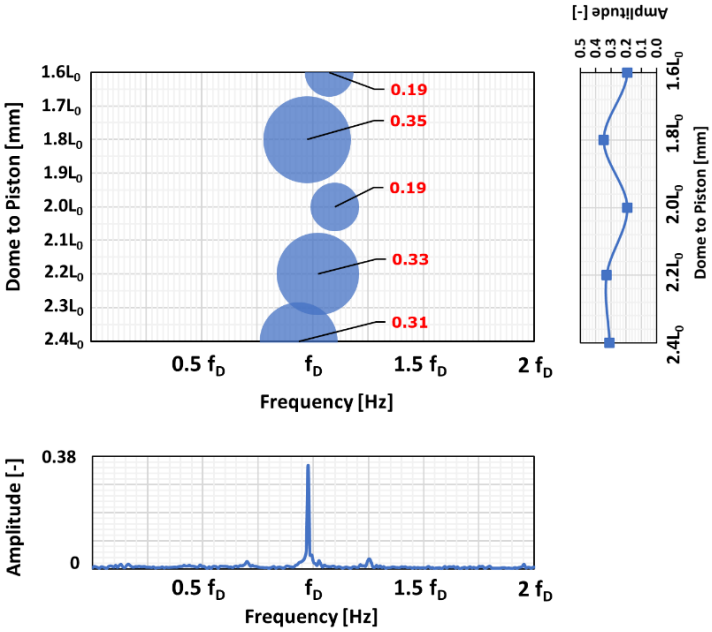

Figure 6. *Numerical results for the 5 selected cases. The size of the bubble represents the amplitude of the pressure fluctuation. The FFT in the bottom side of the picture is performed for the case at the highest amplitude with the dome-to-piston distance of $1.8L_0$. On the right side, the graph reports the trend of the amplitude as a function of the flame tube length.*

Analysis of the numerical results for the case with the highest acoustic amplitude

In this section, the attention will be focused more closely to the case having the dome-to-piston distance equal to $1.8L_0$ where the pressure fluctuation peak is reached. Figure 7 reports the post-processing of the acoustic pressure signal acquired inside the primary zone, approximately at the same position where the experimental probe is located. The pressure fluctuation here reported includes the growth ramp till the limit cycle saturation.

The spectrograph of the signal, showing the time evolution of both the dominant frequency and the amplitude, reveals that no other frequency is excited in any phase of the simulation. The time window analysis highlights that during the ramp there is a slight change of the dominant frequency, moving from $1.03\ f_D$ to the final value of $0.97\ f_D$. In both graphs, it can be noticed that the limit cycle condition is reached approximately after 80 ms, despite the presence of a typical overshot of the acoustic pressure. This kind of post-processing is also useful to better understand when the simulation has reached a steady-state condition and the collection of data at useful locations of the domain can get started.

At this purpose, in order to shed some light on the physical mechanism sustaining the instability, a phase-locked average (PLA) analysis is performed at the same unstable frequency of the self-excited excitation. The data are extracted on a plane showing the fuel injection inside the premixing duct and acquired for at least 25 cycles of the instability. The PLA cycle is split in 14 phases.

Figure 8 reports, for sake of simplicity, only the 4 most significant phases of the PLA cycle: the top of the picture regards the mixture fraction inside the premixer while the bottom the acoustic pressure in the primary zone of the combustor. Looking at the fuel gas concentration, it can be noticed that the jet morphology is influenced by the state of the acoustic pressure in the flame tube. The maximum penetration length in the axial direction is reached during the phase 2, when the combustor is close to the minimum acoustic pressure; similarly, at phase 10, with the combustor experiencing the peak of p', the jet is characterized by the shortest penetration. As a consequence of the oscillation of the fuel plume, the concentration of the mixture at the inlet of the combustor is subjected to fluctuate as well: basing on the length of the premixing duct and the bulk velocity of the mixture, the highest and the lowest mean mixture fraction values are again observed at phase 2 and 10, respectively.

Considering also the convective time that the equivalence ratio fluctuation takes to travel across the primary zone and reach the flame front location (here identified as the center of gravity of the progress variable iso-surface at value of 0.9), the total convective time from the fuel location to the heat release region can be estimated in about 8 PLA phases.

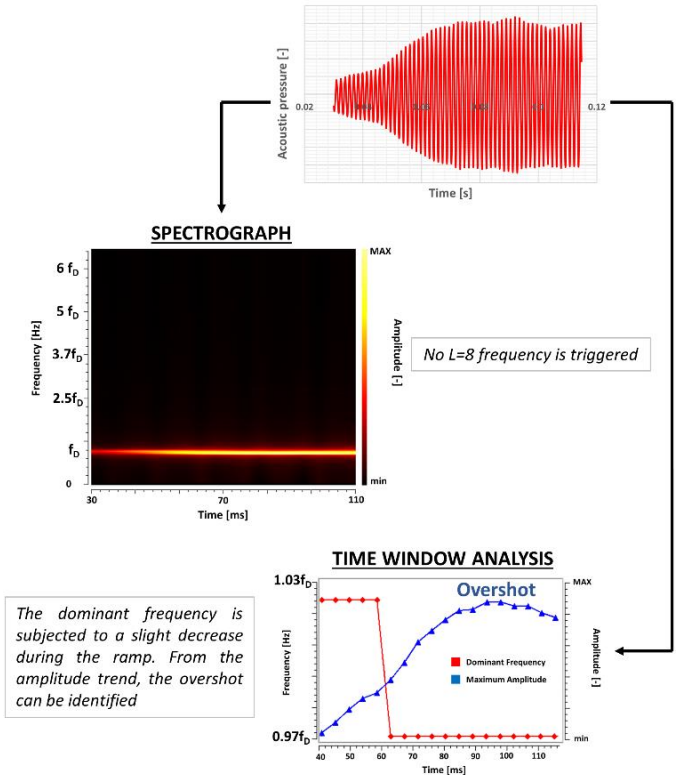

Figure 7. *Spectrograph and time window analysis for the case with flame tube length of $1.8L_0$.*

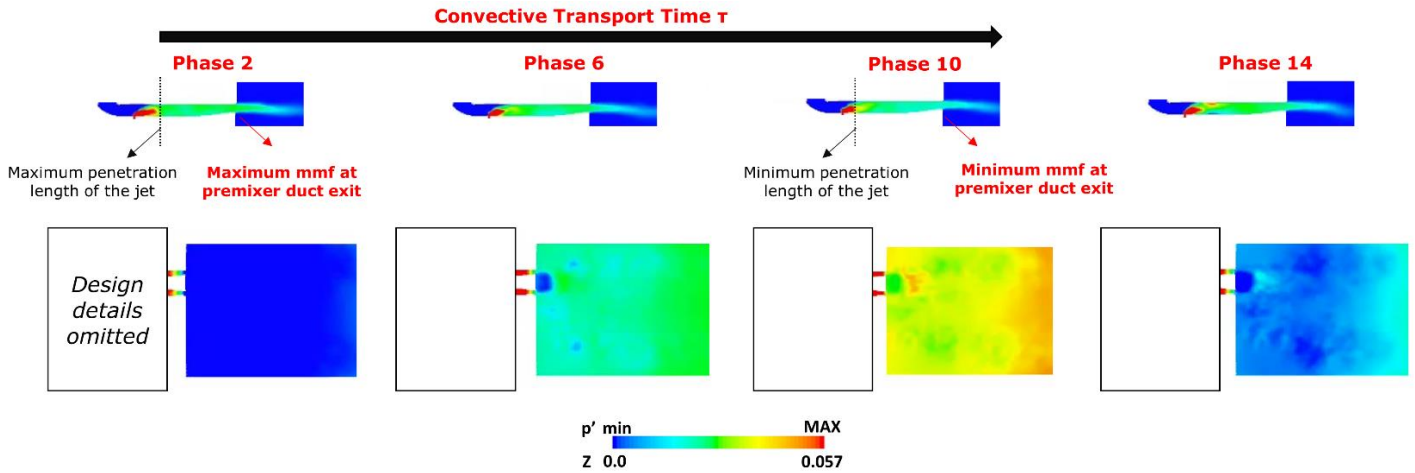

Figure 8. *Phase-Locked Average: the most significant 4 phases out of 14 are here selected for the analysis. Top: mean mixture fraction inside the premixing duct; Bottom: acoustic pressure in the primary zone of the flame tube. The results show that the instability is self-sustained by a convective mechanism of the mixture fraction from the injection point toward the primary zone. The cut plane is selected to show the fuel injection point and isolate one tuber from the others at the same time.*

This means that the positive equivalence ratio fluctuation happening at phase 2 will reach the flame front location during the phase 10, burning when the acoustic pressure is at its own peak. So, it can be stated that the mechanism sustaining the self-excited dynamic is based on the convective time of the equivalence ratio fluctuation.

In addition to the PLA analysis, the Extended POD (EPOD) post processing has been performed. The EPOD is a method to analyze correlated events [39-40], projecting a secondary quantity data set into the POD base computed for a primary quantity [41]. So, the EPOD can be particularly useful to correlate and characterize the flow-flame interaction in the presence of a combustion instability. In this paper, the EPOD is applied to a dataset of 700 snapshots, acquired with a sampling frequency of 33 kHz with the velocity field acting like the primary quantity. To characterize the flame, the OH mass fraction is used since it detects the flame front locations acting like a marker of the heat release zones. Additionally, the same analysis is repeated for the mean mixture fraction to correlate the equivalence ratio fluctuations to the velocity field.
The standard POD applied to the 2D velocity field reveals that about the 33% of the total turbulent kinetic energy is associated to the first mode and the 45% to the first two modes. This means that, for sake of simplicity, the analysis could be limited to the coherent structures associated to these two modes whose contour plots are reported in Figure 9. In the most of cases, the discussion will be here limited to the first mode to be concise. As expected, the FFTs of the time coefficients reveal a peak frequency aligned with the dominant frequency of the pressure fluctuation.
Since the mean flow is subtracted from the data matrix, the colorbar only shows the locations where a positive or negative value of the velocity fluctuation occurs.

Moreover, this kind of analysis doesn't provide any quantitative information about the amplitude of the oscillation since the POD provides only normalized values. To overcome this limitation and quantify the impact of each mode onto the mean flow field, the algebraic sum of the latter quantity plus the temporal evolution of the amplitude of the mode has been considered. The analysis will be here focused on the first POD mode since it can be demonstrated that the same findings that are going to be discussed are valid also for the second one. Figure 10 shows the instants when the sum of the mean flow and the first mode reaches the minimum and the maximum along the cycle.

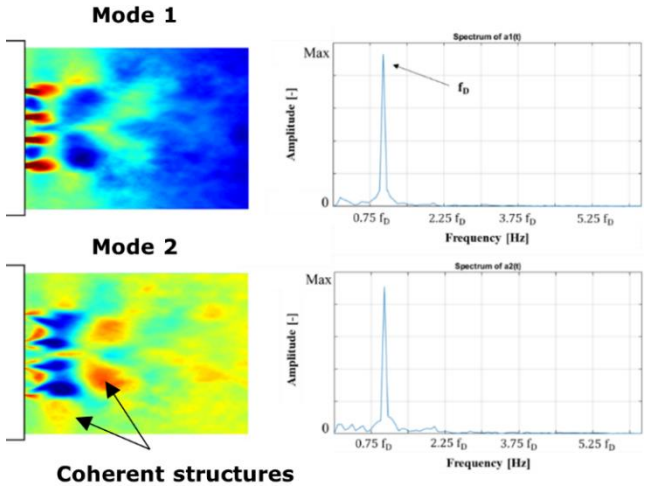

Figure 9. *Axial velocity POD modes and the corresponding frequency content.*

The effect of the first mode onto the mean velocity field results in a shear layer compression toward the premixer exit and in an axial elongation at the instants of the minimum and the maximum fluctuation, respectively. Another major effect of this mode is related to the extension of the recirculation zones. Strong negative velocity regions are identifiable in the outer side of the flame tube when the oscillation cycle of the first mode reaches

its own minimum while quite limited recirculation zones are present at the oscillation peak.

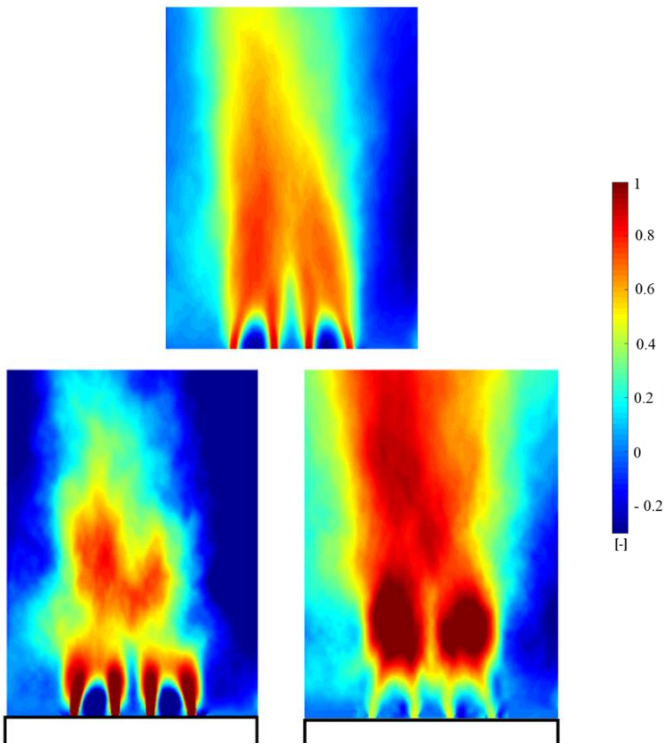

Figure 10. *Mean flow-field (Top) plus first POD mode at the minimum (left) and maximum (right) oscillation level (Bottom). © 2022 Baker Hughes Company - All rights reserved.*

The link between the flow dynamic and the flame fluctuation can be studied through the analysis of the EPOD of the OH mass fraction reported in Figure 11. In terms of frequency content, it can be noticed that the first and second EPOD modes have a peak frequency coincident with the one of the first two axial velocity POD modes and with the dominant frequency of the system. This happens because the EPOD identifies the modes of OH that are correlated to the axial velocity POD modes. So, the first OH EPOD mode represents the OH field structures that are synchronized with the oscillations related to the first axial velocity POD mode.

More importantly, Figure 12 shows the algebraic sum of the OH mean field with its first mode at the instants when the minimum and maximum level of the axial velocity fluctuations are reached.

In both these frames, the regions where the OH has its maxima correspond to low velocity or recirculation zones where the flame gets stabilized. At the minimum fluctuation level, the heat release region is closer to the premixer exit with five major hot spots. Instead, at the maximum oscillation of the axial velocity, the flame can anchor only in the outer recirculation zone of the flame tube with a considerably lower OH mass fraction with respect to the previous instant. So, it can be concluded that the flame stabilization and consequently the heat release rate are strongly dependent on the coherent structures of the velocity field here identified by the first POD mode.

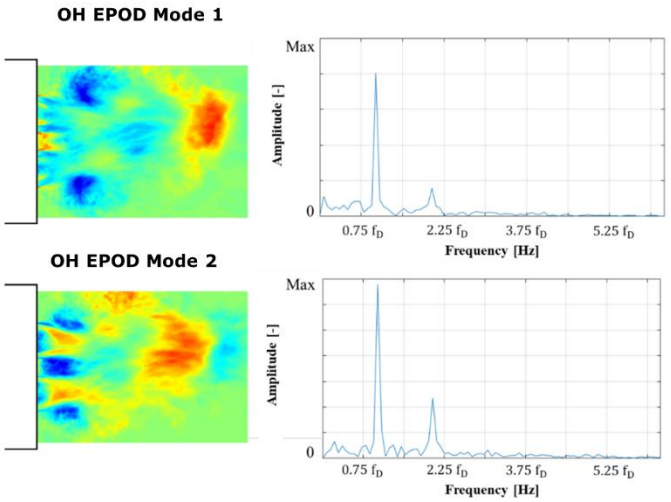

Figure 11. *OH mass fraction first two EPOD modes and the corresponding frequency content. © 2022 Baker Hughes Company - All rights reserved.*

This kind of post processing is also applied to the time average field of the mean mixture fraction, always considering the axial velocity data set as the projection base.

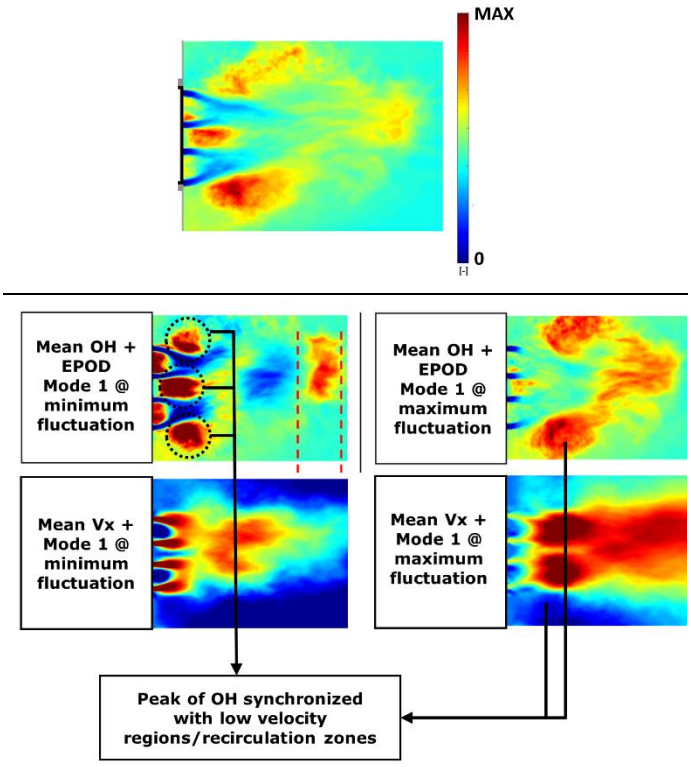

Figure 12. *Top: Time-average OH field. Bottom Left: Mean OH field plus first EPOD modes at the minimum velocity oscillation. Bottom Right: Mean OH field plus first EPOD modes at maximum velocity oscillation (contours are normalized with scale 0 (min) to 1 (max)). © 2022 Baker Hughes Company - All rights reserved.*

From Figure 13 it can be seen that the first two mixture fraction EPOD modes are associated to an axial stretch of the time average equivalence ratio. At the point of their minimum oscillations (Figure 13, left-hand side), leaner mixtures are present at the premixer exits and richer pockets are established downstream in the primary zone. The latter are originated by the convective transport of the high equivalence ratio pockets present at the exit of the premixers at the instants of the Z-EPOD maxima (Figure 13, right-hand side) for the first (top) and the second (bottom) mode, respectively. This is also demonstrated by the fact that the convective time from the burner exit to the heat release region can be roughly estimated in 0.5 ms that is the time interval between the minima and the maxima of these two EPOD modes. This demonstrates once again that the combustion dynamic is driven by the equivalence ratio fluctuation at the burner exit that in turn is strongly correlated with the axial velocity and more specifically with the first POD mode of the axial velocity.

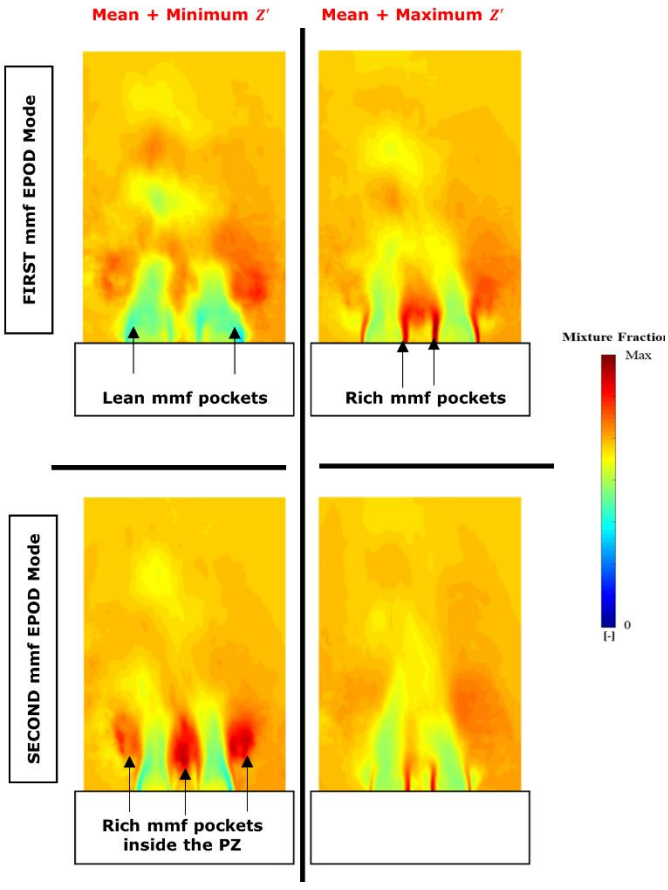

Figure 13. *Top row: First mmf EPOD mode. Bottom row: Second mmf EPOD mode. The column of the left hand side represents the time average + the first EPOD mode at the minimum fluctuation, the right one the same quantity at the maximum fluctuation level. © 2022 Baker Hughes Company - All rights reserved.*

Testing additional flame tube lengths out of the experimental data

Three additional lengths of the flame tube are investigated to verify the behavior of the numerical model outside the range of the experimental data. With the goal to limit the computational effort, shorter dome-to-piston distances are selected, namely $1.0L_0$, $1.2L_0$ and $1.4L_0$.

Figure 13 updates the graph of Figure 5, including the results of the newly simulated conditions. It is confirmed that the dominant frequency remains across the f_D with the third longitudinal mode excited in this case. The dependency of the dominant frequency with respect to the length of the combustor seems to remain unchanged with the slope of the new acoustic island equal to the one of the other cases. The configuration with the flame tube length of $1.0L_0$ is characterized by the lowest pressure fluctuation of the entire numerical campaign: the amplitude of this fluctuation can be considered quite close to noise. The other two configurations are again affected by a significant pressure fluctuation, rising with the flame tube length: the highest level of amplitude is reached also for $1.2L_0$ of the combustor length.

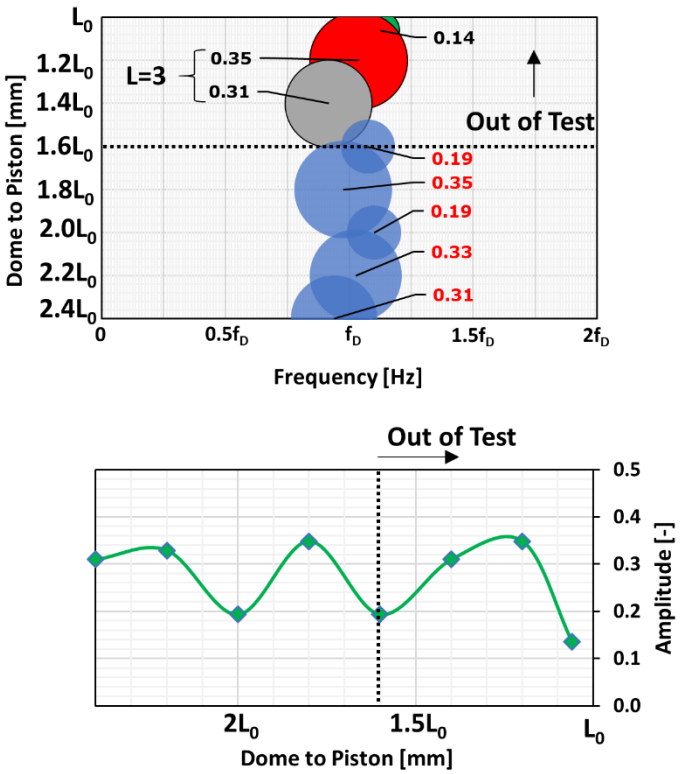

Figure 14. *Numerical findings for the additional three cases simulated for shorter flame tube lengths. The results confirm that the same dominant frequency is excited along the L=3 mode. © 2022 Baker Hughes Company - All rights reserved.*

The new simulated conditions highlight better than the other ones the transition region between the excitation of two adjacent modes ($N = 3$ and $N = 4$ in this particular case). In fact, it can

be observed that there is a range of tube lengths between $1.4L_0$ and $1.6L_0$ where the fluctuation is subjected to a rough decay, from 0.31 to 0.19. The consequent cyclicality is depicted in the bottom picture of Figure 14: the addition of these three cases allows a new amplitude cycle to be observed.

CONCLUSIONS

In the present work, a set of experimental data aiming to characterize a technically premixed burner from the combustion dynamic standpoint has been used for the validation of a LES-based process. The numerical model is able to correctly reproduce the dependency of both the dominant frequency and the amplitude on the length of the flame tube, despite a general under-prediction of the latter parameter. In addition, other different values of the dome-to-piston distances have been considered out of the experimental evidence to verify the repeatability of the results.

A more detailed post-processing of the case showing the highest limit cycle amplitude has been performed: both the phase-locked average and the extended proper orthogonal decomposition techniques have been applied to provide some physical insights about the mechanism driving the thermo-acoustic instability. The PLA has been particularly useful for the correlation of the equivalence ratio fluctuation inside the premixing duct with the acoustic pressure in the combustor. This analysis revealed that the instability is sustained by a convective delay time of the mixture fraction fluctuation toward the flame front location.

The application of the EPOD to the OH mass fraction revealed how much the coherent structures of the velocity field have an impact on the position and the extensions of the heat release rate regions inside the primary zone of the flame tube. Similarly, the EPOD applied to the mixture fraction confirmed that the convective transport mechanisms of the equivalence ratio fluctuation are mainly correlated to the axial velocity fluctuation during the acoustic pressure cycle.

REFERENCES

[1] Lieuwen, T., Torres, H., Johnson, C., Zinn, B.T., *"A Mechanism of Combustion Instability in Lean Premixed Gas Turbine Combustors"*, J. Eng. Gas Turbines Power, Jan 2001, 123(1): 182-189 (8 pages).

[2] Kim, J, Lieuwen, T, Emerson, B, Acharya, V, Wu, D, Mckinney, R, Wang, X, Isono, M., *"High-Frequency Acoustic Mode Identification of Unstable Combustors",* Proceedings of the ASME Turbo Expo, GT2019-91029; 12 pages, Phoenix, Arizona, USA., 2019

[3] Poinsot T, *"Prediction and control of combustion instabilities in real engines"*, Proceedings of the Combustion Institute, Volume 36, Issue 1, pp 1-28, 2017.

[4] Bothien, M. R., Noiray, N., and Schuermans, B., *"Analysis of Azimuthal Thermo-acoustic Modes in Annular Gas Turbine Combustion Chambers", J. Eng. Gas Turbines Power*. June 2015; 137(6).

[5] Romano S., Meloni R., Riccio G., Nassini P.C., Andreini A., *"Modelling of natural gas composition effect on low-NOx burners operation in heavy duty gas turbine"*, J. Eng. Gas Turbines Power , vol. 143, Issue 3, 2021.

[6] Cerutti M., Giannini N., Ceccherini G., Meloni R., Matoni E., Romano C., Riccio G., *"Dry Low NOx Emissions Operability Enhancement of a Heavy-Duty Gas Turbine by means of Fuel Burner Design Development and Testing"*, Proceedings of Asme Turbo Expo, GT2018-76587, Oslo, Norway, 2018.

[7] Sattelmayer T., Polifke W., *"Assessment of methods for the computation of the linear stability of combustors"*, Combustion Science and Technology, Volume 175, Issue 3, Pages 453-476 2010.

[8] Haeringer, M., Fournier, G. J. J., Meindl, M., and Polifke, W. (March 31, 2021). *"A Strategy to Tune Acoustic Terminations of Single-Can Test-Rigs to Mimic Thermoacoustic Behavior of a Full Engine"*, *J. Eng. Gas Turbines Power*. July 2021; 143(7): 071029.

[9] Purwar, N., Meindl, M., and Polifke, W., *"Comparison of Model Order Reduction Methods in Thermoacoustic Stability Analysis."*, J. Eng. Gas Turbines Power, GTP-21-1331, 2021.

[10] Avdonin, A., Javareshkian, A., Polifke, W., *"Prediction of Premixed Flame Dynamics Using Large Eddy Simulation With Tabulated Chemistry and Eulerian Stochastic Fields"*, J. Eng. Gas Turbines Power, 141(11): 111024, 2019.

[11] Fournier, G. J. J., Haeringer, M., Silva, C. F., Polifke, W., *"Low-Order Modeling to Investigate Clusters of Intrinsic Thermoacoustic Modes in Annular Combustors."*, J. Eng. Gas Turbines Power, 143(4): 041025, 2021.

[12] Jaensch S., Merk M., Emmert T., Polifke W., *"Identification of flame transfer functions in the presence of intrinsic thermoacoustic feedback and noise",* Combustion Theory and Modelling 22 (3), 613-634, 2018.

[13] Laera, D., Camporeale, S. M., *"A Weakly Nonlinear Approach Based on a Distributed Flame Describing Function to Study the Combustion Dynamics of a Full-Scale Lean-Premixed Swirled Burner",* J. Eng. Gas Turbines Power, 2017, 139(9): 091501.

[14] Laera, D., Schuller, T., Prieur, K., Durox, D., Camporeale, S.M., Candel, S., *"Flame describing function analysis of spinning and standing modes in an annular combustor and comparison with*

experiments", Combustion and Flame 184, 136-152, 2017.

[15] Schuller, T., Poinsot, T., & Candel, S. "*Dynamics and control of premixed combustion systems based on flame transfer and describing functions"*. Journal of Fluid Mechanics, 894*, 2020.*

[16] Xingsi Han, Jingxuan Li, Aimee S. Morgans, *"Prediction of combustion instability limit cycle oscillations by combining flame describing function simulations with a thermoacoustic network model"*, Combustion and Flame, Volume 162, Issue 10, 2015, Pages 3632-3647.

[17] Jingxuan Li, Yu Xia, Aimee S. Morgans, Xingsi Han, *"Numerical prediction of combustion instability limit cycle oscillations for a combustor with a long flame"*, Combustion and Flame, Volume 185, 2017, Pages 28-43.

[18] Giauque, A., Poinsot, T., Nicoud, F., "Validation of a Flame Transfer Function Reconstruction Method for Complex Turbulent Configurations", 14th AIAA Conference, Vancouver Canada, 2008.

[19] Schimek, S, Göke, S, Schrödinger, C, & Paschereit, CO. *"Flame Transfer Function Measurements With CH4 and H2 Fuel Mixtures at Ultra Wet Conditions in a Swirl Stabilized Premixed Combustor",* Proceedings of the ASME Turbo Expo 2012: Turbine Technical Conference and Exposition. Denmark. June 11–15, 2012.

[20] Lartigue G., Meier U., Bérat C., *"Experimental and numerical investigation of self-excited combustion oscillations in a scaled gas turbine combustor"*, Applied thermal engineering 24.11-12 (2004): 1583-1592.

[21] Franzelli, B., Riber, E., Gicquel, L. Y., and Poinsot, T., *"Large eddy simulation of combustion instabilities in a lean partially premixed swirled flame",* Combustion and flame, 2012, Volume 159, Issue 2.

[22] Iudiciani P., Duwig C., Husseini S.M., Szasz R.Z., Fuchs L., Gutmark E.J., *"Proper Orthogonal Decomposition for Experiemental Investigation of Flame Instabilities",* American Institute of Aeronautics and Astronautics Journal, vol. 50, no. 9, pp. 1843-1854, 2012.

[23] Steinberg A.M., Boxx I., Stöhr M., Carter C.D., Meier W., *"Flow–Flame Interactions Causing Acoustically Coupled Heat Release Fluctuations in a Thermo acoustically Unstable Gas Turbine Model Combustor",* Combustion and Flame, Volume 57, Issue 12, pp. 2250–2266, 2010.

[24] Sieber M., Paschereit O.C., Oberleithner K., *"Advanced Identification of Coherent Structures in Swirl-Stabilized Combustors"*, J. Eng. Gas Turbines Power, Volume 139, Issue 2, 2017.

[25] Kushwaha A., Kasthuri P., Pawar S.A., Sujith R.I., Chterev I., Boxx I., *"Dynamical Characterization of Thermoacoustic Oscillations in a Hydrogen-Enriched Partially Premixed Swirl-Stabilized Methane/Air Combustor.",* J. Eng. Gas Turbines Power*,* GTP-21-1335, 2021.

[26] Huang C., Anderson W.E., Harvazinski M.E., Venkateswaran S., *" Analysis of Self-Excited Combustion Instabilities Using Decomposition Techniques"*, American Institute of Aeronautics and Astronautics Journal, Volume 54, Issue 9, 2016.

[27] Meloni R, Ceccherini G, Michelassi V, Riccio G, "*Analysis of the Self-Excited Dynamics of a Heavy-Duty Annular Combustion Chamber by Large-Eddy Simulation"*, Journal of Engineering for Gas Turbines and Power, vol. 141, Issue 11, 2019.

[28] Laera, D., Campa, G., Camporeale, S.M., Bertolotto, E., Rizzo, S., Bonzani, F., Ferrante, A., *"Modelling of Thermoacoustic Combustion Instabilities Phenomena: Application to an Experimental Rig for Testing Full Scale Burners",* Proceedings of the ASME Turbo Expo 2014, Düsseldorf, Germany, 2014.

[29] Meloni, R., Gori, S., Andreini, A., Nassini, P.C., *"CO Emission Modeling in a Heavy Duty Annular Combustor Operating with Natural Gas"*, J. Eng. Gas Turbines and Power, GTP-21-1375, 2021.

[30] ANSYS, Inc. (2018). ANSYS Fluent Theory Guide, Release 2018.

[31] Van Oijen, J.A., deGoey, L.P.H., *"Modelling of Premixed Laminar Flames using Flamelet-Generated Manifolds"*, Combustion Science and Technology, 161(1), pp. 113–137, 2000.

[32] Zimont, V., Polifke, W., Bettelini, M., Weisenstein, W., *"An Efficient Computational Model for Premixed Turbulent Combustion at High Reynolds Numbers Based on a Turbulent Flame Speed Closure"*, J. of Gas Turbines Power, 120:526-532, 1998.

[33] Zimont, V., Biagioli, F., Syed, K.J., *"Modelling Turbulent Premixed Combustion in the Intermediate Steady Propagation Regime"*, Progress in Computational Fluid Dynamics, 1(1):14-28, 2001.

[34] Goodwin DG, Speth RL, Moat HK, Weber BW, *"Cantera: An object-oriented software toolkit for chemical kinetics, thermodynamics, and transport processes"*, 2018.

[35] S.B. Pope, *"Ten questions concerning the large eddy simulations of turbulent flows"*, New Journal of Physics, Volume 6, 2004

[36] Pope S.B., *"Turbulent Flows"*, *Cambridge University Press*, 2011.

[37] Nassini, P.C., Pampaloni, D., Meloni, R., Andreini, A., *"Lean blow-out prediction in an industrial gas turbine combustor through a LES-based CFD analysis"*, Combustion and Flame, Volume 229, 2021.

[38] Meloni, R., Andreini, A., and Nassini, P. C., *"A Novel LES-Based Process for NOx Emission Assessment in a Premixed Swirl Stabilized Combustion System",* J. Eng. Gas Turbines Power, GTP-21-1374, 2021.

[39] Borée, J. *"Extended proper orthogonal decomposition: a tool to analyse correlated events in turbulent flows"*. Exp Fluids 35, 188–192, 2003.

[40] Maurel, S., Borée, J., Lumley, J.L. *"Extended proper orthogonal decomposition: application to jet/vortex interaction"*. Flow Turb. Combust. 67, 125-136, 2001.

[41] Berkooz, G., Holmes, P. J. Lumley, J. L., *"The Proper Orthogonal Decomposition in the Analysis of Turbulent Flows"*. Annual Review of Fluid Mechanics 25, pp. 539–575, 1993.

